Applied Catalysis B: Environmental 217 (2017) 615–621

Contents lists available at ScienceDirect

Applied Catalysis B: Environmental

journal homepage: www.elsevier.com/locate/apcatb

Highly efficient hydrogen production using p-Si wire arrays and NiMoZn heterojunction photocathodes

Sung Kyu Choi[a,b], Guangxia Piao[a,c], Wonyong Choi[d], Hyunwoong Park[a,b,c,*]

[a] School of Energy Engineering, Kyungpook National University, Daegu 41566, South Korea
[b] Advanced Institute of Water Industry, Kyungpook National University, Daegu 41566, South Korea
[c] School of Architectural, Civil, Environmental, and Energy Engineering, Kyungpook National University, Daegu 41566, South Korea
[d] School of Environmental Science and Engineering, POSTECH, Pohang 37673, South Korea

ARTICLE INFO

Article history:
Received 20 March 2017
Received in revised form 4 May 2017
Accepted 7 June 2017
Available online 8 June 2017

Keywords:
Artificial photosynthesis
Solar fuel
Electrocatalyst
Water splitting
Morphology

ABSTRACT

Highly efficient photoelectrochemical (PEC) hydrogen production is achieved using p-Si wire arrays loaded with NiMoZn particles in aqueous sulfuric acid under simulated sunlight (AM 1.5 G; 100 mW cm^{-2}). Vertically-aligned wire arrays are grown on planar Si wafers via a quick electroless etching process within 5 min, leading to short Si wires of ~4 μm and diameters of ~0.2 μm. Despite the short length of the wires, the reflectance of the arrays is < 5% over the wavelength range of 400–800 nm (the reflectance of planar Si is ~40%) and the photocurrent density (I_{ph}) is enhanced by ~ 30% relative to planar Si. To further improve the PEC performance, ~ 100 nm NiMoZn particles are photoelectrochemically deposited onto the wires. The wire arrays with evenly distributed NiMoZn particles show a photocurrent onset potential (E_{on}) of ~ + 0.27 V vs. RHE and produce an I_{ph} of ~1.45 mA cm^{-2} at 0 V vs. RHE with a Faradaic efficiency of ~ 100% for H_2 evolution. This I_{ph} value is ~10-fold greater than that with the planar Si/NiMoZn samples. The excellent performance of the wire arrays and NiMoZn heterojunction is attributed to enhanced light absorption (decreased reflectance), facilitated charge transfer (radial-directional electron transfer), and NiMoZn-catalyzed hydrogen production.

1. Introduction

Sunlight-driven production of molecular hydrogen (H_2) from water has received growing attention as an alternative to conventional carbon-footprint H_2 production processes (e.g., steam-methane reforming) [1–3]. There are several technical pathways for solar hydrogen production; yet photoelectrochemical (PEC) systems are likely the most viable in terms of synthesis and material modification, system installation, evolved gas separation (e.g., H_2 and O_2), and hybridization with conventional photovoltaics. Despite this great potential, PEC devices suffer from low efficiency, stability, and durability, as well as high costs of the electrode materials [4–7]. Particularly, low efficiency often results from the slow kinetics of charge carriers at the electrode/electrolyte interface [8–11].

p-Type silicon (Si) is widely used as the photocathode in PEC devices because of its narrow bandgap (E_g ~1.2 eV) and suitable band level for the hydrogen evolution reaction (HER) [12,13]. However, the mirror-like planar surface of Si reflects a significant fraction of incident photons. In addition, the small absorption coefficient of Si requires a thick film in order to absorb more photons; however, the short diffusion length of the minority carriers causes significant bulk recombination [14,15]. A wire-array geometry of Si has been demonstrated to possess superior antireflection property capable of absorbing ~96% of the solar photons over a wide range of incident angles [16]. In addition, the photogenerated minority carriers in the bulk can be radial-directionally transported to the electrolyte [14]. Furthermore, wire geometries with a high surface roughness can provide a better environment to tailor the particle size of the loaded catalysts [17].

Despite these morphological effects, the catalytic property (i.e., the interfacial electron injection efficiency) remains mostly unchanged, and HER catalysts are required for prompt electron injection. In contrast to traditional platinum group metals, transition metal alloys (Ni-Mo [18] and Ni-Zr [19]), sulfides (MoS_2 [20] and NiS_2 [21]), phosphides (Ni_2P [22] and CoP [23]), and nitrides (WN and TiN [24]) have been developed as earth-abundant element-based catalysts. The interstitial metal alloys can tune the proton binding energy (ΔG_H) to the metal surface by adjusting the electronic structure of the metal, leading to an optimal ΔG_H and a reduction in the HER overpotential [19,25]. For instance, the intro-

* Corresponding author at: School of Architectural, Civil, Environmental, and Energy Engineering, Kyungpook National University, Daegu 41566, South Korea.
E-mail address: hwp@knu.ac.kr (H. Park).

http://dx.doi.org/10.1016/j.apcatb.2017.06.020
0926-3373/

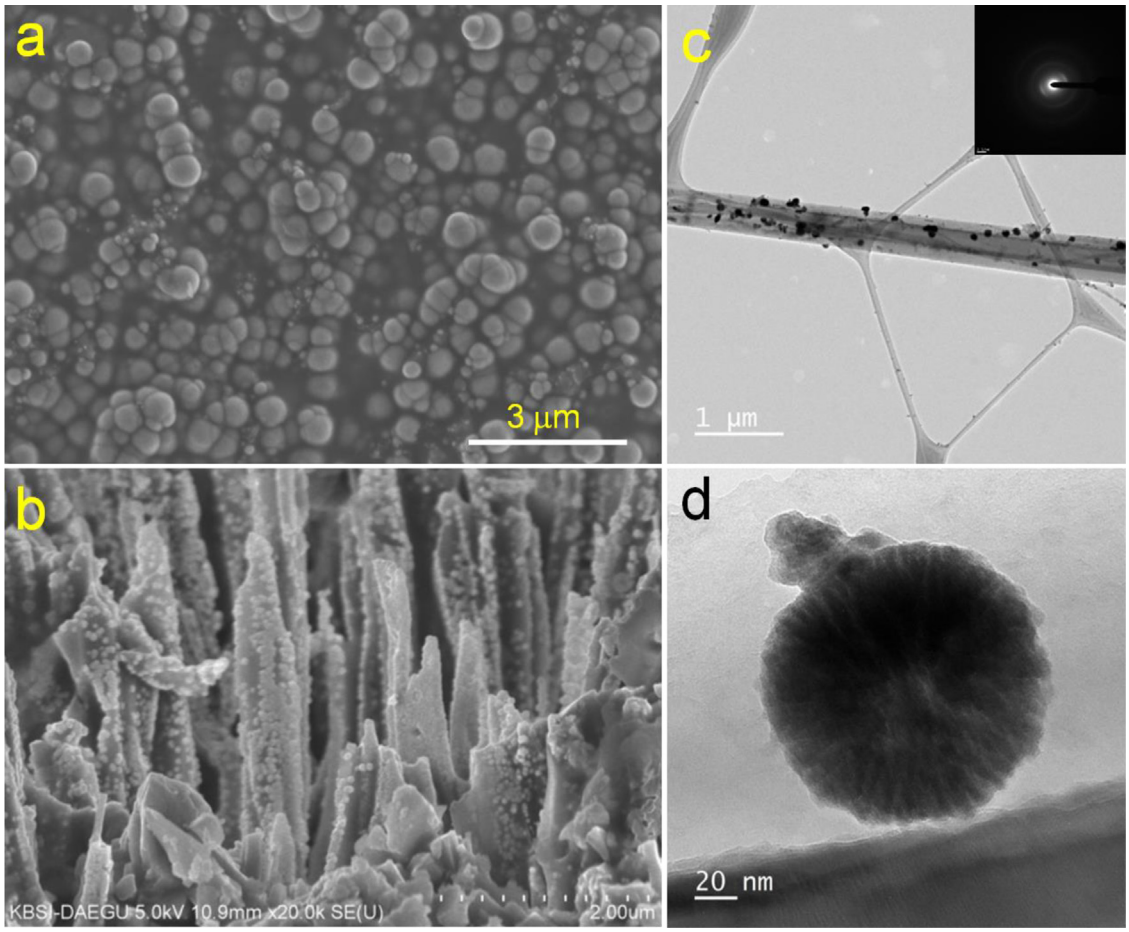

Fig. 1. SEM images of (a) the top view of planar Si and (b) the cross-sectional view of the Si wire arrays deposited with NiMoZn particles for 5 min. TEM images of (c) a Si wire deposited with NiMoZn (Inset: SAED pattern of NiMoZn) and (d) a magnified view of a NiMoZn particle.

duction of Mo into Ni has been shown to modify the electron density states of the *d* orbitals, thereby changing the ΔG_H on the metal surface [26,27]. Further, the addition of trace Zn to NiMo optimized the physicochemical properties, leading to a dramatic improvement in the HER [28].

With this in mind, we synthesized the p-Si wire arrays deposited with NiMoZn particles and examined the PEC hydrogen production in an aqueous sulfuric acid solution under AM 1.5 G light (100 mW cm^{-2}). Vertically aligned, free-standing p-Si wire arrays grew quickly on p-Si wafers via an electroless chemical etching process. In contrast to previous studies with 15–140 μm long wires, short wires (~4 μm) were synthesized because of their superior anti-reflectivity (< 5% in the wavelength range of 400–800 nm). NiMoZn particles were then deposited onto the wire arrays under a constant current for 5 min while irradiating with simulated sunlight. Despite the short synthetic process, the loading of NiMoZn significantly improved the photocurrent density of bare p-Si wire arrays by ~10 times at 0 V vs. RHE while achieving ~100% Faradaic efficiency for the HER. The as-synthesized wire arrays coupled with NiMoZn were characterized with various analytical tools and the NiMoZn-catalyzed HER was discussed in detail.

2. Experimental section

2.1. Synthesis of p-Si wire arrays and NiMoZn heterojunction

Unless otherwise specified, all chemicals and reagents were purchased from Sigma-Aldrich and used without any pretreatment. The Si wire arrays were prepared using an Ag-catalyzed electroless chemical etching method with *p*-type Si (100) wafers (WaferKorea, Inc.; B-doped at 10^{14}–10^{16} cm^{-3} based on its resistivity of 1–30 Ω cm according to the manufacturer's information). The Si wafer was washed with acetone, 2-propanol, and then ultrapure deionized water (>18 MΩ cm, Human Corporation). The back side of the Si wafer was sealed with Teflon tape to block contact with the Ag particles. The native Si surface oxides were removed by sequential cleansing with a piranha solution (i.e., 95% H_2SO_4/30% H_2O_2, 3:1 (v/v)) and a 5% HF solution. Ag seed particles were deposited on the Si wafer using aqueous solutions of $AgNO_3$ (10 mM, 99.8%, Duksan) and HF (5 M) for 3 min, which was then rinsed with deionized water. After the Ag particle deposition step, electroless chemical etching was performed in an aqueous mixed solution of H_2O_2 (0.27 M) and HF (5 M) for 5 min to grow the wire arrays. Then, the as-synthesized samples were soaked in 65% HNO_3 to remove the residual Ag particles, rinsed with deionized water, and dried in an N_2 stream.

The wire-arrayed Si wafers were cut into pieces onto which a silver paste (Cans, Inc.) was painted to create an ohmic contact with the back side. Following drying at 80 °C, the Si wafers were masked with epoxy (Loctite 1C Hysol) over an area of 0.2 cm^2 exposed to the electrolyte. NiMoZn particles were photoelectrochemically deposited from a mixed solution of $NiCl_2{\cdot}6H_2O$ (10 mM, 98%), Na_2MoO_4 $2H_2O$ (5 mM, 99%), $ZnCl_2$ (0.1 mM, 97%), $Na_4P_2O_7$ (30 mM, 99%), $NaHCO_3$ (200 mM, 99%), and hydrazine hydrate (1 mL/L, 98%). The Si samples were immersed in the plating solution and biased at a negative current of 5 mA cm^{-2}, typically for 5 min under AM 1.5 G irradiation at 100 mW cm^{-2} (150 W Xe-arc lamp, ABET Technologies).

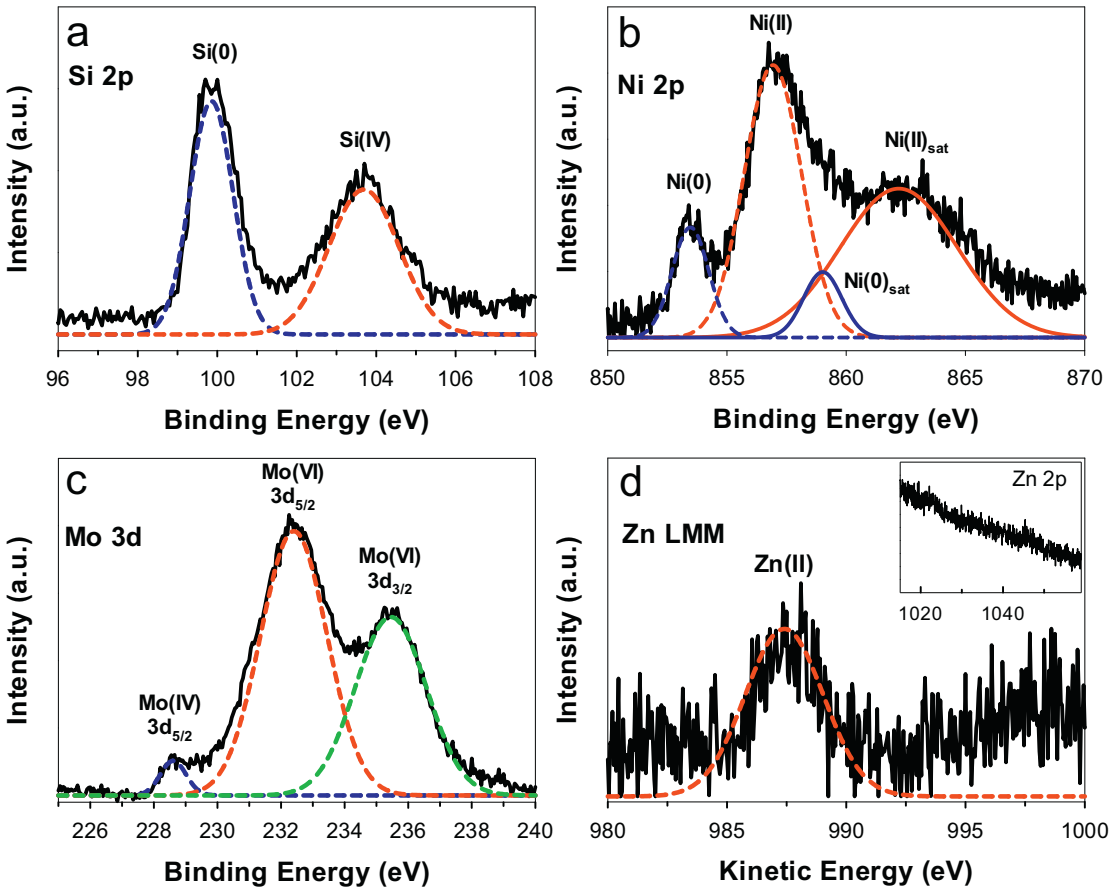

Fig. 2. High-resolution XPS spectra of Si wire arrays deposited with NiMoZn: (a) Si, (b) Ni 2p, (c) Mo 3d, and (d) Zn LMM Auger spectrum (Inset: Zn 2p spectrum). The original spectra (solid lines) were deconvoluted (dashed lines).

2.2. Photoelectrochemical measurements

The photoelectrochemical behavior of the Si samples (working electrode) was examined in 0.5 M sulfuric acid with the saturated calomel electrode (SCE, reference electrode) and a Pt wire (counter electrode) under AM 1.5 G irradiation (100 mW cm^{-2}). The electrolyte was purged with N_2 gas for 1 h to remove dissolved and headspace oxygen in an air-tight single glass cell with a rubber stopper. All (photo)electrochemical measurements were conducted by a potentiostat (Ivium). Potentials were swept from 0.2 V to −1.5 V vs. SCE at a scan rate of 50 mV s^{-1}. Electrochemical impedance spectroscopy (EIS) was performed to obtain the Mott-Schottky plots with a frequency range from 0.1 Hz to 2 kHz in 0.5 M sulfuric acid. For the Nyquist plots, alternating current (AC) impedance measurements were carried out through the application of a bias potential from 0 to −0.4 V vs. SCE in 0.5 M sulfuric acid with a frequency range from 10 MHz to 0.01 Hz and an AC voltage of 10 mV under AM 1.5 G irradiation (100 mW cm^{-2}). All obtained potential values were converted to the reversible hydrogen electrode (RHE) potential using the following equation: $V_{RHE} = V_{SCE} + 0.241\ V + 0.059 \times pH$. Hereafter, the notation "RHE" was omitted for simplicity unless otherwise mentioned. The amounts of hydrogen evolved at 0 V_{RHE} were quantified by injecting the headspace gas into a gas chromatograph (GC, Young Lin, ACME-6100) equipped with a thermal conductivity detector (TCD) and a molecular sieve column (5 Å). Faradaic efficiencies for H_2 were estimated using following equation: H_2 [moles] × 2 × F × 100%/(I × t), where I, t, and F are the current [A], time [s], and the Faraday constant [96,485 C mol^{-1}], respectively.

2.3. Surface characterization

The top and cross-sectional images of bare and modified Si samples (planar and wire arrays with NiMoZn) were acquired using field emission scanning electron microscopy (FE-SEM, Hitachi S-4800) and high-resolution transmission electron microscopy (HR-TEM) equipped with an energy dispersive X-ray (EDX) detector for elemental mapping. An X-ray photoelectron spectrometer (XPS, VG scientific, ESCA LAB 220i XL) with the Mg-Kα line ($h\nu$ = 1253.6 eV) as the X-ray source and an Auger spectrometer (Zn LMM; XPS, ULVAC-PHI, PHI 700) with the Al-Kα line ($h\nu$ = 1486.6 eV) were employed to examine the oxidation states of individual components.

3. Results and discussion

3.1. Surface characterization of wire arrays deposited with NiMoZn

The SEM images of the chemically etched Si samples show the unique morphology of vertical-aligned, free-standing wire arrays with wire lengths of 3–4 μm and an inter-wire distance of ~100 nm (Figs. 1 and S1). This morphology was produced via an etching process using Ag nanoparticles that penetrate the wafer in the presence of H_2O_2/HF. Clearly, the morphology of the wire arrays can be influenced by the etching time and the density of the Ag particles. Typically, the wires grow gradually with etching time and the Ag particle size determines the inter-wire distance. For example, etching times of 1 h and 10 h generated wires that

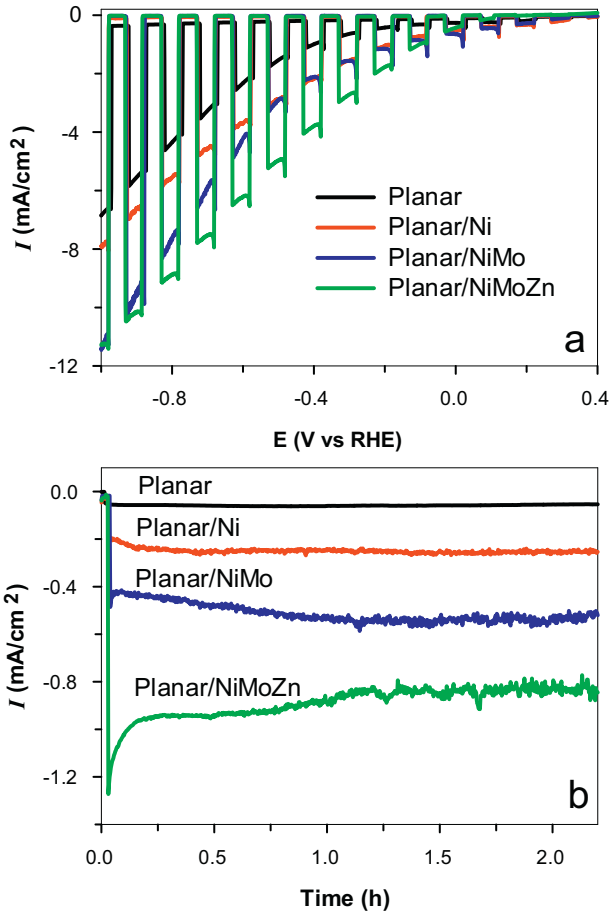

Fig. 3. (a) Chopped linear sweep voltammograms and (b) Time-profiled photocurrents (at −0.1 V vs. RHE) of planar Si samples deposited with Ni, NiMo, and NiMoZn in 0.5 M H_2SO_4 under AM 1.5 G (100 mW·cm^{-2}).

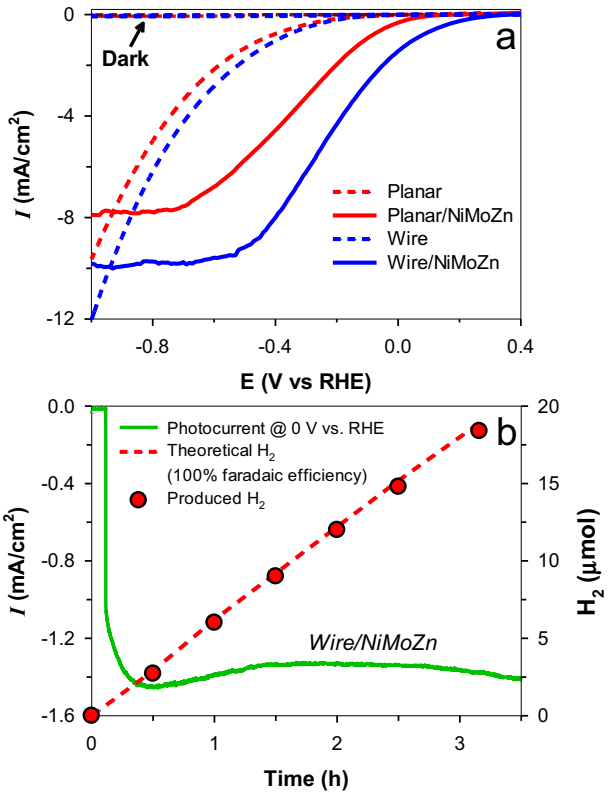

Fig. 4. (a) Linear sweep voltammograms of p-Si planar and wire arrays without and with NiMoZn in 0.5 M H_2SO_4 under AM 1.5 G (100 mW cm^{-2}). (b) Time-profiled photocurrent generation and simultaneous H_2 evolution on p-Si wire arrays coupled with NiMoZn at 0 V vs. RHE in 0.5 M H_2SO_4 under AM 1.5 G (100 mW·cm^{-2}).

were ~15 μm and ~140 μm long, respectively, with a fixed wire diameter of ~100 nm [29]. In this study, the Si wafers were etched for only 5 min to obtain short wire arrays (3–4 μm).

Subsequently, NiMoZn particles were photoeletrochemically deposited onto the planar (i.e., non-etched samples) and wire array Si samples in a mixed solution of Ni, Mo, and Zn under a constant cathodic current of 5 mA cm^{-2} (Fig. 1). It was found that the NiMoZn particles on the planar Si substrate grew to ~1 μm rapidly (<5 min) and then became interconnected into a type of film as the deposition time increased to 10 min, before finally peeling off from the surface (data not shown). The NiMoZn particles deposited onto the wire arrays for 5 min were ~100 nm in size and found only on the wire surface (Fig. 1). The NiMoZn particles became larger (~1 μm) with a deposition time of 10 min, completely filling the inter-wire space and covering the top surface (Fig. S2). TEM analysis of the NiMoZn deposited onto the wire arrays indicated mean particle diameters of ~100 ± 10 nm, and the selected-area electron diffraction patterns further revealed an amorphous structure (Fig. 1c). The EDX elemental mapping analysis clearly showed that the deposited particles are composed of ~20% Ni, ~15% Mo, and ~1% Zn (Fig. S3).

Fig. 2 shows the XPS analysis of the NiMoZn deposited onto the wire arrays for 5 min. The Si 2p spectrum showed a mixed state of Si(0) and Si(IV) (Fig. 2a). The former originated from the Si bulk, whereas the latter is attributed to native SiO_2 and/or formed SiO_2 during the electrochemical deposition of NiMoZn in aqueous solution. The Ni 2p spectrum showed a satellite band at ~861 eV and two Ni-associated bands; deconvolution of the latter band revealed the coexistence of the Ni^0 state at 853.3 eV and the Ni^{2+} state at 856.9 eV (Fig. 2b). The latter appeared to be related to $Ni(OH)_2$. In the case of the Mo 2p spectrum, three Mo-associated bands were found, which were resolved into Mo^{4+} at 228.6 eV and mixed Mo^{6+} states at 232.4 eV ($3d_{5/2}$) and 235.4 eV ($3d_{3/2}$) (Fig. 2c). However, the Zn 2p band was not found in the deposited samples. Instead, the Zn LMM Auger transition revealed a kinetic energy peak at 987.5 eV, which is associated with Zn^{2+} (Fig. 2d). These data clearly indicate that the deposited particles existed as mixed oxides composed of Ni, Mo, and Zn [28]. The XPS analysis revealed that the deposited NiMoZn particles are composed of ~21% Ni (Ni^0/Ni^{2+} = 2/3), ~17% Mo (Mo^{4+}/Mo^{6+} = 1/6.7), and ~0.8% Zn (Zn^{2+} = 1), the composition of which is very similar to the ratio estimated by EDX (Table S1).

3.2. Photoelectrochemical behavior and performance

Fig. 3a compares chopped linear sweep voltammograms (LSVs) of planar Si electrodes (bare and modified with Ni, NiMo, and NiMoZn) in aqueous sulfuric acid (0.5 M) under AM 1.5G irradiation (100 mW cm^{-2}). It should be noted that Ni and NiMo are well known HER catalysts, whereas NiMoZn has received less attention [28]. Relative to bare Si the photocurrent onset potentials (E_{on}) shifted positively by the deposition of Ni and NiMo. It is noteworthy that the incorporation of a tiny amount of Zn (1 atomic%) significantly enhanced the photocurrent density (I_{ph}) of planar Si/NiMo, leading to a stable cathodic I_{ph} of > 0.8 mA cm^{-2} at −0.1 V over 2 h (Fig. 3b). This value is greater than those of planar Si with Ni and NiMo, which suggests that Zn plays a crucial role in enhancing the electrocatalytic performance of NiMo. The introduction of Mo into Ni was reported to modify the binding energy of hydrogen (ΔG_H) on the metal surface, whereas the addition of trace Zn could adjust the oxidation states and aggregation of the particles [28]. When elec-

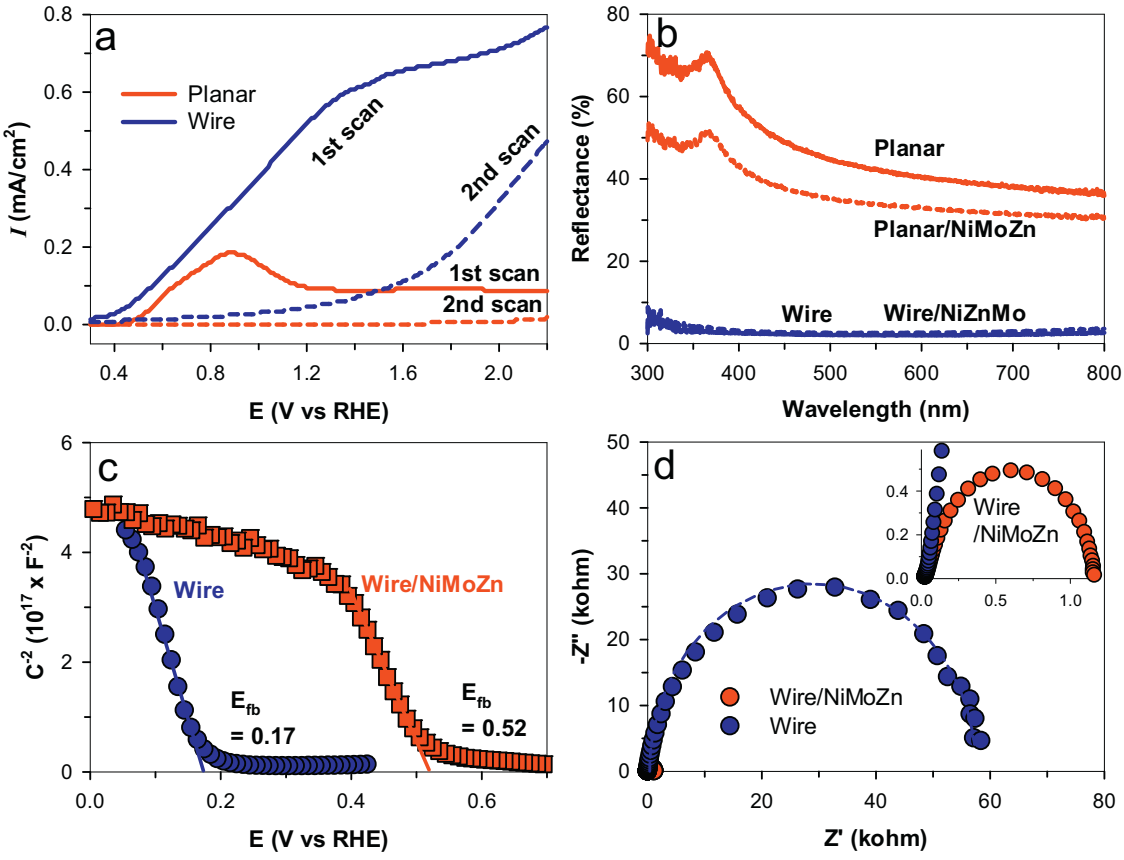

Fig. 5. (a) Repeated anodic potential scans of Si planar and wire arrays from +0.3 V to +2.2 V (solid lines: first scan, dashed lines: second scan). (b) UV–vis reflectance of Si planar and wire arrays without (solid lines) and with (dashed lines) NiMoZn. (c) Mott-Schottky plots of Si wire arrays without and with NiMoZn. (b) Nyquist plots of Si wire arrays without and with NiMoZn under AM 1.5 G irradiation at 0 V vs. SCE. Inset: magnified plots in the high-frequency region.

trochemically deposited on a metal substrate (Ni foil), NiMoZn was found to work effectively for electrocatalytic HER (Fig. S4). Clearly, the deposition of NiMoZn shifted the onset potential by +400 mV, leading to the H_2 production with the Faradaic efficiency of ~100%.

The PEC behavior of the planar and wire arrays (without and with the NiMoZn deposition) was further examined in aqueous sulfuric acid (0.5 M) under AM 1.5G irradiation (100 mW cm^{-2}). The planar Si samples showed an E_{on} at ca. −0.2 V and the deposition of NiMoZn shifted the E_{on} to ~0.1 V (Fig. 4a). This change of 0.3 V in E_{on} by the metal particles was similarly observed for p-Si deposited with Sn and TiN [24,29]. The Si wire arrays exhibited an E_{on} similar to that of planar Si and a slightly enhanced I_{ph} (~1.4 and ~1.8 mA cm^{-2} at −0.5 V for the planar and wire arrays, respectively). Considering the short wires, the photocurrent enhancement most likely resulted from facilitated charge transfer via a radial direction and/or enhanced light absorption (*see below*). The NiMoZn deposition onto the wire arrays shifted the E_{on} by ~0.5 V (from −0.2 V to +0.3 V), significantly enhancing the I_{ph} value (Fig. 4a). It should be noted that the planar and wire arrays with NiMoZn exhibited more positive E_{on} than 0 V (HER potential) and they could produce photocurrents at 0 V (i.e., I_{ph} of ~0.14 and ~1.45 mA cm^{-2} at 0 V for the Si planar and wire arrays, respectively). Accordingly, the planar and wire arrays deposited with NiMoZn were further compared for their PEC H_2 production at 0 V under AM 1.5G irradiation (Fig. 4b). The planar Si/NiMoZn sample generated insignificant I_{ph} (~0.06 mA cm^{-2}) under a constant potential of 0 V and no measurable amount of H_2 was found (data not shown). In contrast, the wire arrays/NiMoZn generated a stable I_{ph} of ~1.4 mA cm^{-2} at 0 V over 3.5 h while producing H_2 at a Faradaic efficiency of ~100%.

3.3. Uniqueness of the heterojunction Si wire arrays and NiMoZn

The enhanced PEC performance of the p-Si wire arrays deposited with NiMoZn can be attributed to the following effects. First, the wire array configuration increases the surface roughness (γ) to provide a better environment for NiMoZn particle growth and an enlarged solid/solution interface. The surface roughness is proportional to the degree of the Si surface exposed to the electrolyte; hence, we performed anodic potential scans for Si oxidation to quantify the actual value of the surface roughness [30]. As shown in Fig. 5a, the first anodic scan of the planar Si generated a current at E > ~0.45 V with a peak at ~0.9 V. However, there was no measurable current in the second scan. Given that the exposed Si surface is readily oxidized in the first scan (e.g., $Si + 2H_2O \rightarrow SiO_2 + 4H^+ + 4e^-$, $E^\circ = -0.91$ V), the near zero current in the second scan indicates that virtually the entire Si surface in direct contact with the electrolyte is fully oxidized to insulating silicon oxides/hydroxide. The wire arrays exhibited similar behavior (i.e., a current decrease in the second scan). However, the oxidation peak position was delayed to ~1.3 V and the magnitude of the current was significantly greater compared with the planar Si. Furthermore, an anodic current was still generated even in the second scan. Assuming that the current in the first scan is attributed to the mixed currents for Si oxidation and for other electrochemical reactions and that the current in the second scan is associated with other electrochemical reactions, the current difference between the first and second scans should be attributed solely to Si oxidation. The charges used for Si oxidation with the planar and wire arrays were estimated to be ~1.78 and ~6.83 mC cm^{-2}, respectively. This indicates that γ of the wire arrays is ~3.8-times larger than that of planar Si. Due to this large γ, the

wire arrays should provide an ample surface for the uniform deposition of ~100 nm-sized NiMoZn particles while inhibiting particle aggregation [31].

The second unique feature of the Si wire arrays deposited with NiMoZn is the reduced anti-reflectivity. As shown in Fig. 5b, planar Si exhibited reflectance of 40–70% in the wavelength range between 300 and 800 nm. The deposition of NiMoZn slightly decreased the reflectance, presumably because of re-absorption of scattered photons by the NiMoZn particles. In contrast, the reflectance of the wire arrays was <5% across the entire wavelength range, indicating that the re-absorption effect of scattered photons is significant. The as-observed reflectance of 3–4 μm-long wires was much smaller than those of longer wires (~15 μm) that were physically synthesized [24]. The deposition of NiMoZn insignificantly changed the reflectance because of virtually full absorption by the wire arrays themselves. Accordingly, the primary role of the wire configuration was to enhance light absorption, with no contribution from NiMoZn.

The effects of NiMoZn deposition onto the wire arrays were further examined via electrochemical impedance spectroscopy (Fig. 5c). The flat band potential (E_{fb}) of the wire arrays was estimated to be 0.17 V, which increased to 0.52 V following NiMoZn deposition. Considering the vicinity (<0.2 V) between E_{on} and E_{fb} [32], this positive shift of E_{fb} by NiMoZn agrees qualitatively well with the NiMoZn-induced positive shift of E_{on} (Fig. 4a). This shift appears to be associated with a change in the Helmholtz layer potential drop (V_H) at the solid/solution interface (Eq. (1), where E_F refers to the Fermi level). Note that V_H depends on the point of zero charges (pH_{PZC}) of the materials in solution (Eq. (2)) [33].

$$E_{fb} = E_F + V_H - 4.5 \quad (1)$$

$$V_H = 0.059(pH_{PZC} - pH) \quad (2)$$

The pH_{PZC} of silicon is ~2 [34]. Although the pH_{PZC} of NiMoZn is not available in the literature, it can be presumed to be greater than that of silicon because the pH_{PZC} values of NiO, MoO_3, and ZnO are 6.4–9.1 [35], 6.25 [36], and 6.9–9.8 [35], respectively. In this regard, the anodic shift of E_{fb} of the wire arrays by NiMoZn deposition can be attributed to the large pH_{PZC} of NiMoZn.

Finally, the Nyquist plots of the bare and NiMoZn-deposited wire arrays were obtained to examine the effect of NiMoZn on the charge transfer resistance (R_{ct}) under AM 1.5G irradiation (100 mW cm^{-2}) (Figs. 5 d and S5). The obtained plots showed typical semicircle behavior, and hence they were fitted to a Randles circuit consisting of solution resistance (R_s), double-layer capacitance (C_{dl}), and R_{ct}. The fitting resulted in R_{ct} values of 7.77×10^4 Ω and 4.43×10^3 Ω for the bare wire arrays and the NiMoZn-deposited wire arrays, respectively. The significant decrease in the R_{ct} by NiMoZn was similarly found at various potentials (−0.4 to 0 V vs. SCE) (Fig. S5). This result indicates that NiMoZn reduced the charge transfer resistance of the wire arrays by increasing the electrical conductivity, which facilitated the HER.

4. Conclusions

We have demonstrated that NiMoZn significantly improved the photoelectrochemical performance of p-Si wire arrays in terms of E_{on}, I_{ph}, and the Faradaic efficiency of H_2 evolution. Although the synthesis time of the wire arrays was quick (~5 min) and the wires were short (3–4 μm), the effect of wire configuration was profound such that the reflectance decreased by >8 times and the I_{ph} increased by ~30% relative to planar Si. The rapid deposition of NiMoZn further enhanced the performance of the wire arrays, leading to an I_{ph} of ~1.45 mA cm^{-2} at 0 V vs. RHE with a Faradaic efficiency of ~100% for H_2 evolution. This I_{ph} value was ~10-fold greater than that with planar Si/NiMoZn. The excellent performance of the p-Si wire arrays/NiMoZn heterojunctions was attributed to enhanced light absorption (decreased reflectance), facilitated charge transfer (radial-directional electron transfer), and NiMoZn-catalyzed hydrogen production. Given the low cost of the required elements (Si, Ni, Mo, and Zn), the easy availability of p-Si wafers, and the quick synthesis time (total 10 min), the p-Si wire array/NiMoZn heterojunction described herein has great potential application in several relevant fields.

Acknowledgments

This research was supported by the Global Research Network Program (2014S1A2A2027802), Basic Science Research Program (2016R1A2B4007366), and Global Research Laboratory Program (2014K1A1A2041044), Korea. In addition, we are grateful to the Korea CCS R&D Center (KCRC) (No. 2014M1A8A1049354) for financial support.

Appendix A. Supplementary data

Supplementary data associated with this article can be found, in the online version, at http://dx.doi.org/10.1016/j.apcatb.2017.06.020.

References

[1] K. Maeda, K. Domen, Photocatalytic water splitting: recent progress and future challenges, J. Phys. Chem. Lett. 1 (2010) 2655–2661.
[2] H.-J. Lewerenz, L. Peter, Photoelectrochemical Water Splitting: Materials, Processes and Architectures, The Royal Society of Chemistry, Cambridge, 2013.
[3] H. Park, H.I. Kim, G.H. Moon, W. Choi, Photoinduced charge transfer processes in solar photocatalysis based on modified TiO_2, Energy Environ. Sci. 9 (2016) 411–433.
[4] F.E. Osterloh, Inorganic nanostructures for photoelectrochemical and photocatalytic water splitting, Chem. Soc. Rev. 42 (2013) 2294–2320.
[5] U. Kang, S.K. Choi, D.J. Ham, S.M. Ji, W. Choi, D.S. Han, A. Abdel-Wahabe, H. Park, Photosynthesis of formate from CO_2 and water at 1% energy efficiency via copper iron oxide catalysis, Energy Environ. Sci. 8 (2015) 2638–2643.
[6] N.C. Deb Nath, S.Y. Choi, H.W. Jeong, J.J. Lee, H. Park, Stand-alone photoconversion of carbon dioxide on copper oxide wire arrays powered by tungsten trioxide/dye-sensitized solar cell dual absorbers, Nano Energy 25 (2016) 51–59.
[7] U. Kang, H. Park, A facile synthesis of $CuFeO_2$ and CuO composite photocatalyst films for the production of liquid formate from CO_2 and water over a month, J. Mater. Chem. A 5 (2017) 2123–2131.
[8] T.H. Jeon, W. Choi, H. Park, Cobalt-phosphate complexes catalyze the photoelectrochemical water oxidation of $BiVO_4$ electrodes, Phys. Chem. Chem. Phys. 13 (2011) 21392–21401.
[9] S.K. Choi, W. Choi, H. Park, Solar water oxidation using nickel-borate coupled $BiVO_4$ photoelectrodes, Phys. Chem. Chem. Phys. 15 (2013) 6499–6507.
[10] H.W. Jeong, T.H. Jeon, J.S. Jang, W. Choi, H. Park, Strategic modification of $BiVO_4$ for improving photoelectrochemical water oxidation performance, J. Phys. Chem. C 117 (2013) 9104–9112.
[11] S.Y. Choi, C.-D. Kim, D.S. Han, H. Park, Facilitating hole transfer on electrochemically synthesized p-type $CuAlO_2$ films for efficient solar hydrogen production from water, J. Mater. Chem. A (2017), http://dx.doi.org/10.1039/C1037TA01919J.
[12] X.G. Zhang, Electrochemistry of Silicon and Its Oxide, Kluwer Academic/Plenum, New York, 2001.
[13] D.M. Andoshe, S. Choi, Y.S. Shim, S.H. Lee, Y. Kim, C.W. Moon, D.H. Kim, S.Y. Lee, T. Kim, H.K. Park, M.G. Lee, J.M. Jeon, K.T. Nam, M. Kim, J.K. Kim, J. Oh, H.W. Jang, A wafer-scale antireflective protection layer of solution-processed TiO_2 nanorods for high performance silicon-based water splitting photocathodes, J. Mater. Chem. A 4 (2016) 9477–9485.
[14] B.M. Kayes, H.A. Atwater, N.S. Lewis, Comparison of the device physics principles of planar and radial p-n junction nanorod solar cells, J. Appl. Phys. 97 (2005).
[15] H.W. Jeong, W.S. Chae, B. Song, C.H. Cho, S.H. Baek, Y. Park, H. Park, Optical resonance and charge transfer behavior of patterned WO_3 microdisc arrays, Energy Environ. Sci. 9 (2016) 3143–3150.
[16] J.Y. Jung, M.J. Choi, K. Zhou, X. Li, S.W. Jee, H.D. Um, M.J. Park, K.T. Park, J.H. Bang, J.H. Lee, Photoelectrochemical water splitting employing a tapered silicon nanohole array, J. Mater. Chem. A 2 (2014) 833–842.
[17] S.Q. Liu, Z.R. Tang, Y.G. Sun, J.C. Colmenares, Y.J. Xu, One-dimension-based spatially ordered architectures for solar energy conversion, Chem. Soc. Rev. 44 (2015) 5053–5075.

[18] J.M. Jakšić, M.V. Vojnović, N.V. Krstajić, Kinetic analysis of hydrogen evolution at Ni-Mo alloy electrodes, Electrochim. Acta 45 (2000) 4151–4158.
[19] M. Metikoš-Huković, A. Jukić, Correlation of electronic structure and catalytic activity of Zr-Ni amorphous alloys for the hydrogen evolution reaction, Electrochim. Acta 45 (2000) 4159–4170.
[20] D.W. Redman, H.J. Kim, K.J. Stevenson, M.J. Rose, Photo-assisted electrodeposition of MoS:X from ionic liquids on organic-functionalized silicon photoelectrodes for H_2 generation, J. Mater. Chem. A 4 (2016) 7027–7035.
[21] D. Kong, J.J. Cha, H. Wang, H.R. Lee, Y. Cui, First-row transition metal dichalcogenide catalysts for hydrogen evolution reaction, Energy Environ. Sci. 6 (2013) 3553–3558.
[22] E.J. Popczun, J.R. McKone, C.G. Read, A.J. Biacchi, A.M. Wiltrout, N.S. Lewis, R.E. Schaak, Nanostructured nickel phosphide as an electrocatalyst for the hydrogen evolution reaction, J. Am. Chem. Soc. 135 (2013) 9267–9270.
[23] Z. Huang, Z. Chen, C. Lv, M.G. Humphrey, C. Zhang, Cobalt phosphide nanorods as an efficient electrocatalyst for the hydrogen evolution reaction, Nano Energy 9 (2014) 373–382.
[24] S.K. Choi, W.S. Chae, B. Song, C.H. Cho, J. Choi, D.S. Han, W. Choi, H. Park, Photoelectrochemical hydrogen production on silicon microwire arrays overlaid with ultrathin titanium nitride, J. Mater. Chem. A 4 (2016) 14008–14016.
[25] A. Metikos-Hukovic, Z. Grubac, N. Radic, A. Tonejc, Sputter deposited nanocrystalline Ni and Ni-W films as catalysts for hydrogen evolution, J. Mol. Catal. A-Chem. 249 (2006) 172–180.
[26] S. Martinez, M. Metikos-Hukovic, L. Valek, Electrocatalytic properties of electrodeposited Ni-15Mo cathodes for the HER in acid solutions: synergistic electronic effect, J. Mol. Catal. A-Chem. 245 (2006) 114–121.
[27] A. Damian, S. Omanovic, Ni and Ni-Mo hydrogen evolution electrocatalysts electrodeposited in a polyaniline matrix, J. Power Sources 158 (2006) 464–476.
[28] X. Wang, R. Su, H. Aslan, J. Kibsgaard, S. Wendt, L. Meng, M. Dong, Y. Huang, F. Besenbacher, Tweaking the composition of NiMoZn alloy electrocatalyst for enhanced hydrogen evolution reaction performance, Nano Energy 12 (2015) 9–18.
[29] S.K. Choi, U. Kang, S. Lee, D.J. Ham, S.M. Ji, H. Park, Sn-coupled p-Si nanowire arrays for solar formate production from CO_2, Adv. Energy Mater. 4 (2014) 1301614.
[30] I. Oh, J. Kye, S. Hwang, Enhanced photoelectrochemical hydrogen production from silicon nanowire array photocathode, Nano Lett. 12 (2012) 298–302.
[31] K.Q. Peng, X. Wang, X.L. Wu, S.T. Lee, Platinum nanoparticle decorated silicon nanowires for efficient solar energy conversion, Nano Lett. 9 (2009) 3704–3709.
[32] T. Kim, K.S. Choi, Nanoporous $BiVO_4$ photoanodes with dual-layer oxygen evolution catalysts for solar water splitting, Science 343 (2014) 990–994.
[33] A.J. Nozik, Photoelectrochemistry: applications to solar energy conversion, Annu. Rev. Phys. Chem. (1978) 189–222.
[34] M. Kosmulski, IEP as a parameter characterizing the pH-dependent surface charging of materials other than metal oxides, Adv. Colloid Interface Sci. 171 (2012) 77–86.
[35] M. Kosmulski, Isoelectric points and points of zero charge of metal (hydr)oxides: 50 years after Parks' review, Adv. Colloid Interface Sci. 238 (2016) 1–61.
[36] F.J. Gilllambias, A.M. Escudeycastro, Use of zero point charge measurements in determining the apparent surface coverage of molybdena in MoO_3/g-Al_2O_3 catalysts, J. Chem. Soc.-Chem. Commun. (1982) 478–479.